Journal of Applied Electrochemistry **29**: 1171–1176, 1999.

Ni–Zn–P alloy deposition from sulfate bath: inhibitory effect of zinc

M. BOUANANI[1], F. CHERKAOUI[1], M. CHERKAOUI[1]*, S. BELCADI[1], R. FRATESI[2]** and G. ROVENTI[2]
[1]*Laboratoire d'Electrochimie et de Chimie Analytique, Faculté des Sciences, Université Mohammed V. Avenue Ibn Battouta B.P 1014, Rabat, Morocco;* [2]*Dipartimento di Scienze dei Materiali e della Terra, Università degli Studi di Ancona, Via Brecce Bianche, 60131 Ancona, Italy*
**Also at the Université Ibn Tofail, Faculté des Sciences, Kénitra, Morocco*
*(** author for correspondence, fax: +39 71 2204714)*

Received 14 March 1998; accepted in revised form 31 July 1998

Key words: alloys, cyclic voltammetry, electrodeposition, electroless deposition, nickel, phosphorus, zinc

Abstract

Electroless Ni–Zn–P alloy deposition from a sulphate bath, containing sodium hypophosphite as reducer, was investigated. To increase the plating rate, the deposition parameters were optimized. The effect of process parameters (T, pH and $[Zn^{2+}]$) on the plating rate and deposit composition was examined and it was found that the presence of zinc in the bath has an inhibitory effect on the alloy deposition. As a consequence, the percentage of zinc in the electroless Ni–Zn–P alloys never reaches high values. Using cyclic voltammetry the electrodeposition mechanism of Ni–Zn–P alloys was investigated. It was observed that the zinc deposition inhibits the nickel discharge and, as a consequence, its catalytic activity on hypophosphite oxidation. It was also found that increase in temperature or pH leads to the deposition of nickel rich alloys.

1. Introduction

Electrodeposition of Ni–Zn alloys has attracted much interest over the past decade for many applications such as the corrosion protection of steel in vehicles [1–5]. Recently, it was shown that the inclusion of phosphorus, a nonmetallic element, in these alloys can modify their microstructure during electrodeposition and improve their corrosion resistance [6, 7]. However, the electrochemical study of Ni–Zn–P alloys has still not been completely developed.

Other investigations [8, 9] have been devoted to the electroless deposition of these alloys with hypophosphite as reducer and as source of phosphorus in the deposit, because it can be applied as a uniform layer by simple immersion in the plating solution. These alloys are of relevance to the automobile industry as protective coatings. Electroless Ni–Zn–P alloys have been studied only from chloride baths [8, 9] similar to those used by Fischer to deposit thin Co–Zn–P ternary alloy films [10].

In the present work the electroless deposition and the electrodeposition of Ni–Zn–P alloys from sulphate bath were studied to investigate the inhibitory effect of zinc, which affects both processes. In the electroless deposition the effect of experimental parameters (T, pH and $[Zn^{2+}]$) on the plating rate and on the composition of the alloys was studied. Electrochemical investigations on the Ni–Zn–P electrodeposition were performed by means of cyclic voltammetry.

2. Experimental details

Ni–Zn–P alloys were electrolessly deposited using a bath of the following composition: $NiSO_4.6\,H_2O$ 27 g dm^{-3} (0.1 M); $ZnSO_4.7\,H_2O$ 2.9 g dm^{-3} (0.01 M); $NaH_2PO_2.H_2O$ 32 g dm^{-3} (0.30 M); $C_6H_5Na_3O_7.2\,H_2O$ 59 g dm^{-3}; $(NH_4)_2SO_4$ 27 g dm^{-3} and lactic acid 10 g dm^{-3}. The temperature was 90 °C and the pH was adjusted to 9.0 by addition of sodium hydroxide. The solution was prepared with doubly distilled water and analytical grade reagents. This bath was chosen after some preliminary investigations on the chemical stability in order to avoid precipitation or spontaneous decomposition of the solution and to optimize the plating rate. The effect of temperature (from 50 to 90 °C), nickel concentration (from 0.01 to 0.10 M) and zinc concentration (from 0.005 to 0.10 M) were investigated. It was found that the addition of lactic acid enables acceleration of the plating rate by about 55%. The pH was varied between 6.0 and 11.2 by addition of sodium hydroxide. All the solutions were deaerated by nitrogen bubbling. The depositions were obtained on Armco iron sheets of 3 cm^2 surface area. These were mechanically polished and chemically etched in dilute sulphuric acid before the experiments. The plating rate was calculated from sample weight gains. The analysis of the deposits was performed by means of inductively coupled plasma spectroscopy (ICPS).

The cyclic voltammograms were performed from the same baths used for electroless deposition by means of a Tacussel potentiostat PGS 201T monitored by Prolinea 4/50 microcomputer with a Elcom 201 software. The experiments were carried out with different process parameters. The working electrode was vitreous carbon with 0.049 cm^2 surface area. It was selected as substrate because it has a wide domain of electroactivity. The auxiliary electrode was a large area platinum plate (1 cm^2) and the reference electrode was a saturated calomel electrode (SCE). The scan rate was 5 mV s^{-1}.

3. Results and discussions

3.1. *Effect of different plating parameters (T, pH and [Zn^{2+}]) on electroless Ni–Zn–P alloy deposition*

The bath temperature is one of the most important factors affecting the rate of electroless alloy deposition [11]; thus, the deposition rate was determined at temperatures between 50 and 90 °C (pH 9). It was found that no metal deposition occurs at temperature values lower than 60 °C and that the deposition rate is low until 80 °C, while a high deposition rate, without spontaneous decomposition of the bath, is obtained at 90 °C (Table 1); no changes in deposit composition were found at different temperatures.

The effect of pH on plating rate and deposit composition is shown in Figure 1. Above pH 8 the deposition rate increases markedly, in accordance with findings of other authors for Ni–P electroless deposition [12, 13]. The percentage of phosphorus in the deposits decreases with increasing pH and similar behavior was observed by other authors for Ni–P, Co–P [14] and Ni–Zn–P alloys [8, 9].

Most of the investigations on electroless deposition have been carried out in the presence of hypophosphite as reducer, and have shown that hypophosphite oxidation is the dominant factor in the electroless process [15, 16]. In alkaline media [17], according to Pourbaix diagrams [18], the oxidation of hypophosphite is

$$H_2PO_2^- + 3\,OH^- \rightleftharpoons HPO_3^{2-} + 2\,e^- + 2\,H_2O \qquad (1)$$

The incorporation of phosphorus in the deposit results from the disproportionation of $H_2PO_2^-$:

$$3\,H_2PO_2^- \rightleftharpoons 2\,P_{ads} + HPO_3^{2-} + OH^- + 2\,H_2O \qquad (2)$$

Table 1. Effect of temperature on deposition rate and on the composition of deposits

T/°C	v/mg cm^{-2} h^{-1}	Ni/%	Zn/%	P/%
60	0.23	76.6	12.0	11.4
70	0.32	75.8	12.6	11.6
80	0.52	75.9	12.4	11.7
90	0.98	76.8	11.4	11.8

[Ni^{2+}] 0.1 M; [Zn^{2+}] 0.01 M; [$H_2PO_2^-$] 0.3 M; pH 9.0.

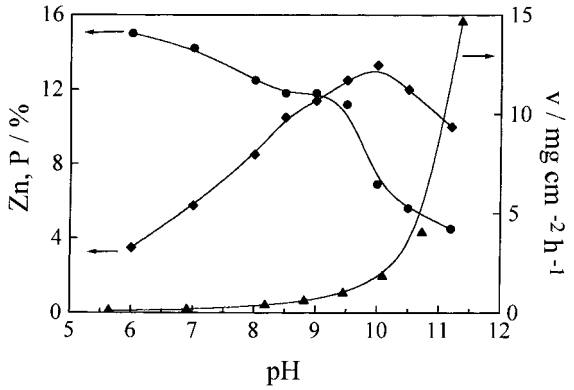

Fig. 1. Effect of pH on the deposition rate (▲), on the percentage of Zn (◆) and P (●) of the deposits. [Zn^{2+}] 0.01 M; [Ni^{2+}] 0.1 M; [$H_2PO_2^-$] 0.3 M; *T* 90 °C.

When the pH value increases, according to Reactions 1 and 2, the rate of hypophosphite oxidation also increases (1) and so the plating rate is accelerated [19], but the amount of incorporated phosphorus is reduced (2). Moreover, the zinc content in the deposit increases from 3.5 to 13.3% when the pH value is varied from 6.0 to 10.0 (Figure 1).

The effect of zinc concentration on the alloy deposition was also studied (Figure 2). It was found that the presence of zinc in the electroless nickel bath strongly affects the plating rate. Indeed, the rate drastically decreases as the zinc content in the bath increases. These results show an inhibitory effect of zinc on the deposition rate of electroless Ni–Zn–P alloys. In addition, the Figure shows that the zinc and phosphorus contents in the deposit change in an opposite sense: that is, on increasing the zinc concentration in the bath, the phosphorus content decreases.

3.2. *Cyclic voltammetry*

Voltammetric investigations were carried out at different conditions to characterize the various oxido-reduction processes and investigate the inhibitory effect of zinc on the Ni–Zn–P alloy electrodeposition.

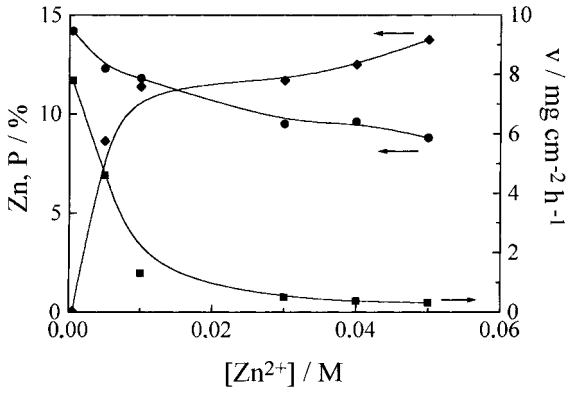

Fig. 2. Effect of zinc concentration on rate deposition (▲), on percentage of Zn (◆) and P (●) of the deposits. [Ni^{2+}] 0.1 M; [$H_2PO_2^-$] 0.3 M; *T* 90 °C; pH 9.0.

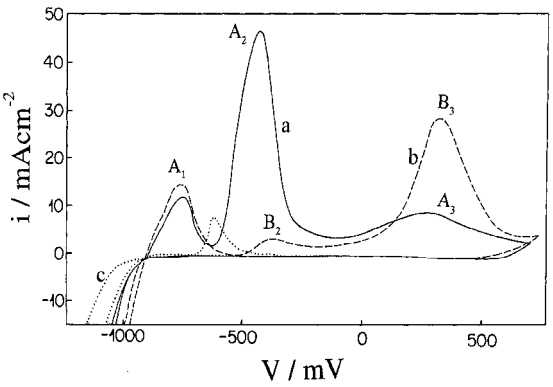

Fig. 3. Cyclic voltammograms obtained on vitreous carbon electrode. (a) Bath containing [Ni^{2+}] 0.1 M; [Zn^{2+}] 0.01 M and [$H_2PO_2^-$] 0.3 M; (b) bath without Zn^{2+}; (c) bath without $H_2PO_2^-$. *T* 90 °C; pH 9.0; 5 mV s^{-1}.

Figure 3 shows the cyclic voltammograms obtained at 5 mV s^{-1} on vitreous carbon. The deposition of the Ni–Zn–P alloy occurs at potentials more negative than about −900 mV (curve (a)) and three oxidation peaks are observed (A_1, A_2 and A_3) in the anodic scan. Peak A_1 is not observed in the hypophosphite free solution (curve (c)) and its intensity increases with the hypophosphite concentration in the bath (Figure 4). Thus, it is associated with the direct oxidation of hypophosphite, as already reported [16]. In the absence of hypophosphite (Figure 3, curve (c)), only one anodic peak and a small hump are observed at −617 and −400 mV, respectively, related to the dissolution of Ni–Zn alloy. Peaks A_2 and A_3 are observed in the complete solution in the same potential region of peaks B_2 and B_3, obtained in the zinc free solution (Figure 3, curve (b)); these peaks were attributed respectively to the dissolution of crystalline and of amorphous Ni–P alloy poor and rich in phosphorus [17, 20, 21], respectively. The increase in peak A_3 with hypophosphite concentration (Figure 4) is due to the increase in phosphorous content in the film and confirms that this peak is associated with the dissolution of amorphous Ni–P alloy rich in phosphorous. It is noteworthy that in the presence of zinc, peak A_2 is broader and higher (Figure 3, curve (a)) probably due to the dissolution of various elements from the same phase. The effect of the process parameters (T, pH, [Ni^{2+}] and [Zn^{2+}]) was examined in order to identify this peak.

Figure 5 shows the voltammograms obtained for various nickel sulphate concentrations. The deposition current at the cathodic value of −1200 mV increases with nickel concentration (Figure 6); this indicates that nickel enhances the alloy deposition and probably the hydrogen evolution, which occurs at low overpotential on nickel. The anodic peak A_1 markedly increases with nickel concentration (Figure 5), showing that hypophosphite oxidation is catalysed by deposition of nickel. The increase in the hypophosphite anodic current with nickel concentration in solution was observed by other authors [22]; it is suggested that a faster electrodeposition of fresh nickel on the substrate from the plating solution is responsible for the higher hypophosphite oxidation current. It has also been shown that nickel has a catalytic activity on the oxidation of hypophosphite in nickel electroless plating [17, 22, 23]. Two peaks, denoted A_2' and A_2'', are observed for nickel concentrations lower than 0.1 M. The intensity of peak A_2'' decreases when the Ni concentration decreases, confirming that it is associated with the oxidation of nickel from the nickel rich α phase. Peak A_2' shifts towards the potential of the peak already reported for the dissolution of Ni–Zn alloy observed at −617 mV (Figure 3, curve (c)), when the Ni^{2+} concentration changes from 0.08 to 0.05 M. The analysis indicates that the composition of the alloy, deposited under potentiostatic conditions at −1200 mV with 0.05 M nickel concentration in solution, is about 32.5% in Zn, 9.1% in P and 58.4 in Ni. The analysis of the deposit obtained under potentiostatic conditions at −1200 mV and then submitted to anodic potentiodynamic stripping up to −550 mV (Figure 5, point X on the curve (c)) shows that the percentage of zinc and phosphorus are about 2.8% and 12% , respectively. This confirms that peak

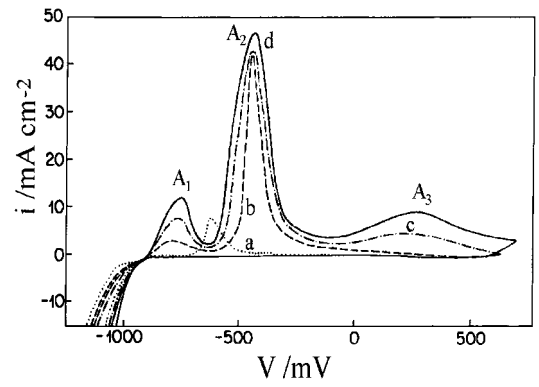

Fig. 4. Cyclic voltammograms obtained at various hypophosphite concentrations: (a) [$H_2PO_2^-$] 0 M; (b) [$H_2PO_2^-$] 0.1 M; (c) [$H_2PO_2^-$] 0.2 M; (d) [$H_2PO_2^-$] 0.3 M. [Zn^{2+}] 0.01 M; [Ni^{2+}] 0.1 M; *T* 90 °C; pH 9.0; 5 mV s^{-1}.

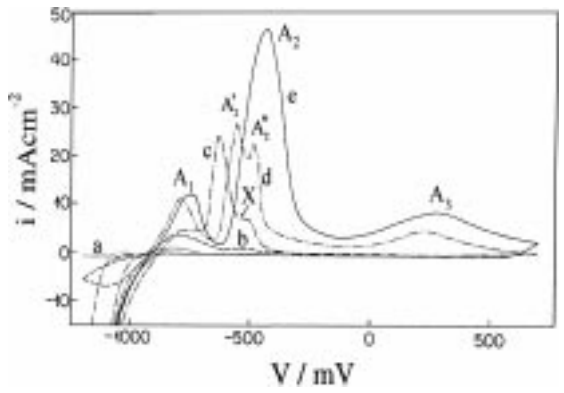

Fig. 5. Cyclic voltammograms obtained at various nickel concentrations: (a) [Ni^{2+}] 0.01 M; (b) [Ni^{2+}] 0.03 M; (c) [Ni^{2+}] 0.05 M; (d) [Ni^{2+}] 0.08 M; (e) [Ni^{2+}] 0.1 M. [Zn^{2+}] 0.01 M; [$H_2PO_2^-$] 0.3 M; *T* 90 °C; pH 9; 5 mV s^{-1}.

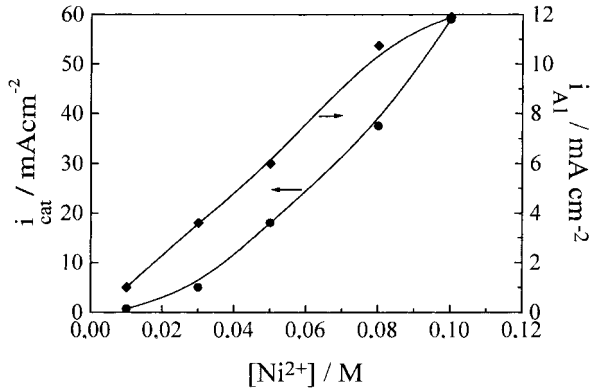

Fig. 6. Deposition current i_{cath} at cathodic inversion potential −1.2 V (●) and anodic peak current of hypophosphite oxidation i_{A1} (◆) at various nickel concentrations. Data from Figure 5.

A_2' is associated with oxidation of zinc from the Ni–Zn α phase. Hence, peak A_2 obtained at the highest concentration of Ni confirms the oxidation of two elements, Zn and Ni, from the same Ni–Zn α phases. On the other hand, it was observed that the percentage of zinc in the alloy decreases from 32.5 to 14.8% when the nickel concentration in solution increases from 0.05 M (curve (c)) to 0.1 M (curve (e)), indicating that the shift of peak A_2' towards a positive potential when the nickel concentration increases is due to the decrease in the percentage of zinc in the deposit. The increase of peak A_3 with nickel concentration confirms that it is related to the formation of an amorphous Ni–P phase [19, 20, 21].

Figure 7 shows the effect of the inversion potential in the range from −1050 to −1200 mV. When the potential is scanned to about −1050 mV and −1100 mV (curves (a) and (b)) peaks A_2' and A_2'' are observed and peak A_2' is higher than peak A_2'', indicating preferential zinc deposition. At −1150 mV (curve (c)) peak A_2' decreases and shifts to a more noble potential. For an inversion potential of −1200 mV (curve (d)) only the broader peak A_2 is observed, indicating a more significant nickel discharge. The increase of peak A_1 with the inversion potential is associated with the increase in hypophosphite oxidation, enhanced by the higher nickel content of the electrodeposits. The increase of peak A_3 indicates a greater electroreduction of nickel and hypophosphite. Table 2 shows the total deposition (Q_d) and oxidation (Q_a) charges calculated by integrating the current/time curves; the current efficiency ($CE = 100 \times Q_a/Q_d$) values are also reported. At the inversion potential of −1200 mV, the current efficiency is above 100% due to an appreciable contribution of the electroless process, more important at this potential. The parallel occurrence of the electroless process in the electrodeposition of Ni–Zn–P alloys was observed by Swathirajan [7] at high temperature and at different current densities. The increase of the contribution of the electroless process is associated with the higher nickel content of the electrodeposits, which enhances the hypophosphite oxidation and thus the electroless process.

Table 2. Total deposition and oxidation charges and current efficiency values for cyclic voltammograms performed at various inversion potential values

V/mV_{SCE}	$Q_d/C\,cm^{-2}$	$Q_a/C\,cm^{-2}$	CE/%
−1050	1.00	0.80	80.0
−1100	1.30	1.10	84.6
−1150	1.60	1.50	93.7
−1200	1.95	2.76	141.5

The effect of temperature is shown in Figure 8. The temperature was increased from 50 to 90 °C. The deposition current at the cathodic limit −1200 mV increases accompanied by a shift of 300 mV in the deposition potential towards more positive values, due to the increase in nickel discharge. At 50 °C the anodic peak related to zinc dissolution from the Ni–Zn α phase rich in nickel (A_2') appears and shifts towards a more positive potential at 70 °C. Increasing the temperature from 70 to 80 °C, peaks A_2' and A_2'' increase. At 90 °C only peak A_2 was observed. This indicates that in the Ni–Zn–P alloy electrodeposition increase in temperature enhances the nickel discharge [24–26]. The intensities of peaks A_1 and A_3 are also increased with temperature, showing a higher hypophosphite oxidation and amorphous Ni–P deposition.

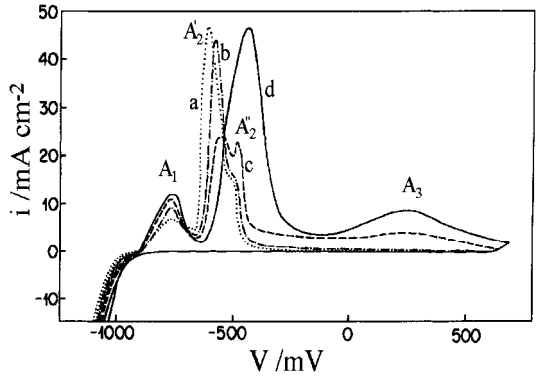

Fig. 7. Cyclic voltammograms obtained at various inversion potential values. (a) −1050 mV; (b) −1100 mV; (c) −1150 mV; (d) −1200 mV. $[Zn^{2+}]$ 0.01 M; $[Ni^{2+}]$ 0.1 M; $[H_2PO_2^-]$ 0.3 M; *T* 90 °C; pH 9.0; 5 mV s^{-1}.

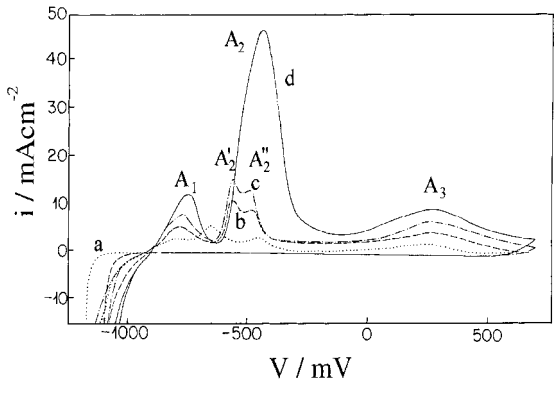

Fig. 8. Cyclic voltammograms obtained at various temperatures: (a) 50 °C; (b) 70 °C; (c) 80 °C; (d) 90 °C. $[Zn^{2+}]$ 0.01 M; $[Ni^{2+}]$ 0.1 M; $[H_2PO_2^-]$ 0.3 M; 5 mV s^{-1}.

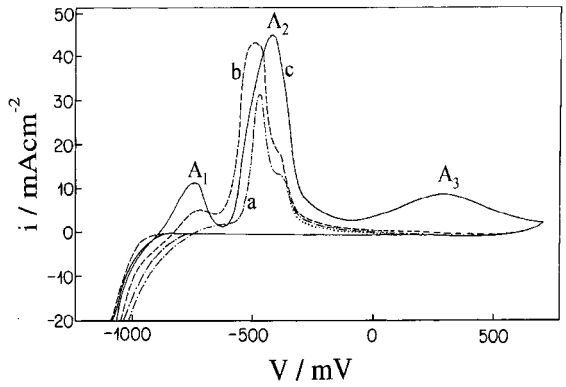

Fig. 9. Cyclic voltammograms obtained at various pH values: (a) pH 6.0; (b) pH 8.0; (c) pH 9.0. $[Zn^{2+}]$ 0.01 M; $[Ni^{2+}]$ 0.1 M; $[H_2PO_2^-]$ 0.3 M; T 90 °C; 5 mV s^{-1}.

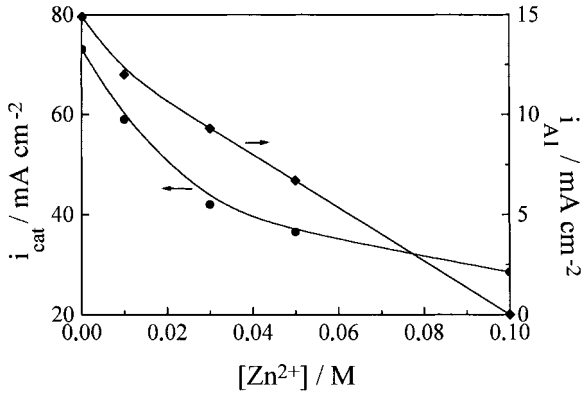

Fig. 11. Deposition current i_{cath} at cathodic limit potential −1.2 V (●) and anodic current of hypophosphite oxidation i_{A1} (◆) at various Zn concentrations. Data from Figure 10.

The effect of electrolyte pH was also examined (Figure 9). The changes in pH do not substantially affect the deposition current at the cathodic limit of −1200 mV, whereas peak A_1 is greatly enhanced when the pH becomes alkaline. This shows that the pH increase promotes hypophosphite oxidation; only a broader single peak A_2 was observed at pH 9, indicating that a low amount of zinc was reduced, as confirmed by the analysis (Zn 14.8%). The increase in peak A_3 with pH is related to the increase in the phosphorous content in the alloy due to hypophosphite electroreduction.

Figure 10 shows the voltammograms obtained for different concentrations of zinc in solution. When the concentration of zinc was increased to 0.01 M, a shift towards less noble potentials with decrease in deposition current at −1200 mV was observed (Figure 11). This indicates the suppression of hydrogen evolution as well as inhibition of nickel discharge. On the reverse scan, the peak A_2 decreases and shifts to more negative potentials when zinc concentration increases from 0.05 to 0.1 M. This is related to the inhibition of nickel discharge by zinc. Peak A_3 decreases indicating a decrease in nickel and phosphorus content in the deposit. The effect of zinc sulphate concentration is very pronounced on hypophosphite oxidation; indeed, the intensity of peak A_1 decreases on increasing the zinc concentration. At 0.1 M zinc this peak is absent, indicating that the hypophosphite oxidation process is strongly inhibited by zinc deposition [27]. These results demonstrate that during Ni–Zn–P alloy electrodeposition, zinc deposits preferentially with inhibition of nickel discharge and, consequently, with depletion of its catalytic activity on hypophosphite oxidation.

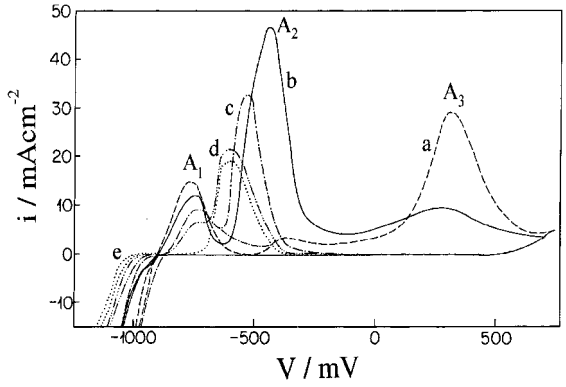

Fig. 10. Cyclic voltammograms obtained at various Zn concentrations. (a) $[Zn^{2+}]$ 0 M; (b) $[Zn^{2+}]$ 0.01 M; (c) $[Zn^{2+}]$ 0.03 M; (d) $[Zn^{2+}]$ 0.05 M; (e) $[Zn^{2+}]$ 0.1 M. $[Ni^{2+}]$ 0.1 M; $[H_2PO_2^-]$ 0.3 M; T 90 °C; pH 9.0; 5 mV s^{-1}.

4. Conclusions

From studies of plating rates and deposit composition in the electroless Ni–Zn–P alloy deposition from sulphate bath in the presence of hypophosphite as reducing agent the following conclusions can be drawn:

(i) No changes in deposit composition were found at different temperatures, but only a change in the plating rate.
(ii) Increase in bath alkalinity favours the codeposition of zinc and nickel.
(iii) The content of phosphorous in the alloy decreases with increase in pH and in zinc concentration.
(iv) The presence of zinc in the bath has an inhibitory effect on alloy deposition, leading to low plating rates. As a consequence, the percentage of zinc in the alloys can never reach high values.

Cyclic voltammetry, carried out with the same bath composition and temperature range of the electroless deposition, leads to the following results:

(i) Increase in temperature or pH favours the electrodeposition of phases rich in nickel.
(ii) Increase in phosphorous content in the alloy with pH is due to the electroreduction of the hypophosphite.
(iii) The electroreduction of nickel enhances hypophosphite oxidation.
(iv) Zinc deposits preferentially with inhibition of nickel discharge and, consequently, with depletion of nickel catalytic activity on hypophosphite oxidation.

Acknowledgement

This work was supported by a cooperation program between Italy and Morocco (projet 03/20/017 soutien à la recherche scientifique au Maroc).

References

1. R. Noumi, H. Nagasaki, Y. Foboh and A. Shibuya, SAE Tech. Pap. Series. No. 820332, Detroit, Michigan (1982).
2. G.F. Hsu, *Plat. Surf. Finish.* **71** (1983) 59.
3. R. Fratesi and G. Roventi, *Surf. Coat. Technol.* **82** (1996) 158.
4. R. Albalat, E. Gómez, C. Müller, J. Pregonas, M. Sarret and E. Vallés, *J. Appl. Electrochem.* **21** (1991) 44.
5. W. Assumus, *Galvanotechnik* **82** (1991) 838.
6. S. Swathirajan and Y.M. Mikhail, *J. Electrochem. Soc.* **136** (1989) 374.
7. S. Swathirajan and Y.M. Mikhail, *J. Electrochem. Soc.* **136** (1989) 2188.
8. D. Snyder, M. Schlesinger and X. Meng, *J. Electrochem. Soc.* **137** (1990) 1858.
9. D. Snyder, M. Schlesinger and X. Meng, *J. Electrochem. Soc.* **138** (1991) 406.
10. R.D. Fisher, *IEEE Trans. Magh.*, Mag- **2** (1966) 681.
11. M. Schwartz, *Proc. Am. Electroplat. Soc.* **47** (1960) 176.
12. A. Brenner and G.E. Riddel, *J. Res. Natl. Bur. Stand.* **37** (1946) 31 *Proc. Am. Electroplat. Soc.* **33** (1946) 23.
13. J.E.A.M. Van Deer Meerakeer, *J. Appl. Electrochem.* **11** (1981) 395.
14. S.L. Chow, N.E. Hedgecok., M. Schlesinger and J. Rezek, *J. Electrochem. Soc.* **119** (1972) 1614.
15. I. Ohmo, O. Wakabayashi and S. Haruyama, *J. Electrochem. Soc.* **132** (1985) 2323.
16. I. Ohmo, *Mater. Sci. Eng. A* **146** (1991) 33.
17. A.H. Gafin and S.W. Orchard, *J. Electrochem. Soc.* **140** (1993) 3458.
18. M. Pourbaix, 'Atlas of Electrochemical Equilibria in Aqueous Solutions' (Pergamon Press, Oxford, 1966), p. 504.
19. M. Bouanani, F. Cherkaoui, M. Cherkaoui, R. Fratesi and G. Roventi, Proceedings of the Second Mediterranean Basin Conference on Analytical Chemistry, Rabat, Maroc (23–28 Nov. 1997), pp. PII-104.
20. J. Crousier, Z. Hanane and J.P. Crousier, *Electrochim. Acta* **38** (1993) 261.
21. L.M. Abrantes and J.P. Correia, *J. Electrochem. Soc.* **141** (1994) 2356.
22. J. Flis and D.J. Duquette, *J. Electrochem. Soc.* **131** (1984) 34.
23. J.H. Marshall, *J. Electrochem. Soc.* **130** (1983) 369.
24. M. Bouanani, F. Cherkaoui and M. Cherkaoui, Proc. Journées d'Electrochimie, Montréal, Canada (2–5 juillet 1997), p. 105.
25. A. Brenner, 'Electrodeposition of Alloys', Vols. I and II (Academic Press. NewYork and London, 1963).
26. L. Felloni, R. Fratesi, E. Quadrini and G. Roventi, *J. Appl. Electrochem.* **17** (1987) 574.
27. M. Bouanani, F. Cherkaoui and M. Cherkaoui, Proc. Second Maghrebian Conference on Process Engineering, Gabés and Djerba, Tunisia (22–25 Apr. 1996), Tome II, 1st part.